Electronic Supplementary Materials (ESI)

Visible-Light-Driven Surface Reconstruction of Mesoporous TiO$_2$: Toward Visible-Light Absorption and Enhanced Photocatalytic Activities

Renhong Li,[a] Hisayoshi Kobayashi*[b] Junfang Guo[a] and Jie Fan*[a]

Material synthesis: Mesoporous TiO$_2$ was prepared by the AcHE process. In a typical synthesis, 10 mmol of Ti(OBu)$_4$, 40 mmol HOAc, 12 mmol HCl (or HNO$_3$), and 1.6 g of F127 (EO$_{96}$PO$_{70}$EO$_{96}$, MW = 12000 g/mol) were dissolved in 30 ml ethanol. The mixture was stirred vigorously for 1 hour and transferred into a Petri dish (diameter 125 mm). The ethanol was evaporated at 40 ^{o}C with a relative humidity of ~ 40%. After 12 hours, a transparent membrane was formed, and it was transferred into a 65 ^{o}C oven and aged for 24 hours. As-synthesized mesostructured hybrids were calcined at 450 ^{o}C in air for 5 hours (ramp rate 2 ^{o}C/min) in order to obtain mesoporous membranes.

VSR-mTiO$_2$ was synthesized as follows: 0.1 mmol benzyl alcohol was added into a suspension of mTiO$_2$ (8 mg/ml) with 5 mL hexane in a quartz tube for 50 h anaerobic photo-oxidation. Side-irradiation by a 300 W high-pressure mercury lamp (an optical filter was adopted to provide visible-light with λ>400 nm) was used to initiate the photoreaction after the tubes bubbling with pure N$_2$ for at least 30 min. Prior to the reactions, GC-TCD was employed to make sure no residual oxygen is present in the tubes. The values of alcohol and product concentration was monitored by GC-FID and calculating the substrate conversion and the selectivity toward aldehyde (toluene was used as the internal standard). The GC results showed that more than 98% benzyl alcohol has been transformed into benzaldehyde after 50 h photoreaction. The residual mTiO$_2$, VSR-mTiO$_2$, was thus extracted by centrifuge and rinsed with water and ethyl alcohol for 3 times, respectively, and then dried at 80 ^{o}C overnight. Other commercial chemicals were of the highest available grade and were used without further purification.

DFT calculation: The band structures for normal and reduced TiO$_2$ surfaces were calculated using the Castep software.[1-2] TiO$_2$ surface was modeled by the (001) face of anatase, and consists of three Ti and six O layers including protruding O atoms on both sides. A Ti$_{12}$O$_{28}$H$_8$ unit cell was used for the normal TiO$_2$ surface. The four O atoms in the bottom layer have one coordination number, and eight H atoms are added to saturate the dangling bonds. Ti$_{12}$O$_{28}$H$_{10}$ and Ti$_{12}$O$_{27}$H$_8$ unit cells were adopted to represent the reduced TiO$_2$ surfaces with hydrogen atoms bonded to oxygen (hydroxyls), and the oxygen vacancy (Ti^{3+} species), respectively. The lattice constants, $a=b=$15.104 Å and $\alpha=\beta=\gamma=90°$ were adopted based on the anatase crystalline data. As to the c direction, the lattice constant was set to 30 Å including the vacuum region. These lattice constants were fixed, and only the atomic coordinates were optimized. The Perdew, Burke and Ernzerhof (PBE) functional[3-4] was used together with the ultra soft core potentials.[5] The basis set cut-off energy was set to 340 eV. The electron configurations of atoms are Ti: 3s^2, 3p^6, 4s^2, 3d^2, O: 2s^2, 2p^4, C: 2s^2, 2p^2, and H: 1s^1.

Material characterization: Low-angle XRD and wide-angle XRD patterns were recorded on a Bruker D8 diffractometer using Cu$_{K\alpha}$ radiation. Transmission electron microscopy (TEM) images

were taken using a JEOL 2010 electron microscope operating at 200 keV. The samples for TEM were prepared by dispersing the final powders in ethanol; the dispersion was then dropped on carbon-copper grids. Nitrogen sorption analysis was carried out at 77K using a Micrometrics TriStar 3000 system. Solid UV/Vis adsorption spectra were measured with a Shimadzu UV-2450 spectrophotometer in the diffuse reflectance mode. XPS measurements were performed in a VG Scientific ESCALAB Mark II spectrometer equipped with two ultra-high vacuum (UHV) chambers. All binding energies were referenced to the C1s peak at 284.8 eV of the surface adventitious carbon. Laser Raman spectra were collected under ambient conditions using an HR LabRaman 800 system equipped with a CCD detector. A green laser beam ($\lambda = 514.5$nm) was used for excitation.

EPR and Spinning Trapping Experiment: X-band EPR signals were recorded at ambient temperature on a Bruker EPR A-300 spectrometer. The settings for the EPR spectrometer were as follows: center field, 3511.39 G; sweep width, 100 G; microwave frequency, 9.86 G; modulation frequency, 100 kHz; power, 101 mW; conversion time, 10msec. The spin trapping experiments were performed as follows: 5,5–Dimethyl-pyrroline-N-oxide (DMPO) spin-trapping reagent and other chemicals were purchased from Sigma-Aldrich Chemical Co. and used without further purification. Stock solutions of DMPO (0.8 M) in deaerated water were prepared under argon and stored in the dark at -20 $^{\circ}$C. The stock DMPO solution was first diluted to 0.08 M with phosphate buffer solution (pH = 7.6) prior to the reaction with any solid substrate. The solid catalyst ($\sim$ 5.0 mg) was mixed with calculated amount of ice-cooled DMPO solution (0.08 M). The mixture was quickly transferred into a glass capillary tube and tested by EPR spectroscopy at room temperature upon visible-light irradiation. A 100 W Hg lamp (LOT Oriel) with an optical filter was used to provide visible-light with $\lambda > 400$ nm.

Photocatalytic experiments: Photocatalytic decomposition of formaldehyde was carried out with 10 mg of photocatalysts suspended in 5 mL of aqueous formaldehyde solution (5.0 vol%) in air using the same reactor as discussed in photo-induced BA oxidation. GC-TCD was employed for evaluating the percentage of mineralization, that is, the amount of CO_2 and H_2. The repeated experimental procedure was as follows: after each 5 h reaction with formaldehyde solution under visible-light irradiation, the reacted solution was centrifuged, and the upper liquid was removed. The residual VSR-$mTiO_2$ was dried at 80 $^{\circ}$ C overnight. The same procedure was repeated for 5 times.

References

1.   M. C. Payne, M. P. Teter, D. C. Allan, T. A. Arias and J. D. Joannopoulos, *Rev. Mod. Phys.*, 1992, **64**, 1045-1097.
2.   V. Milman, B. Winkler, J. A. White, C. J. Pickard, M. C. Payne, E. V. Akhmatskaya and R. H. Nobes, *Int. J. Quantum Chem.*, 2000, **77**, 895-910.
3.   J. P. Perdew, K. Burke and M. Ernzerhof, *Phys. Rev. Lett.*, 1996, **77**, 3865-3868.
4.   J. P. Perdew, K. Burke and M. Ernzerhof, *Phys. Rev. Lett.*, 1997, **78**, 1396-1396.
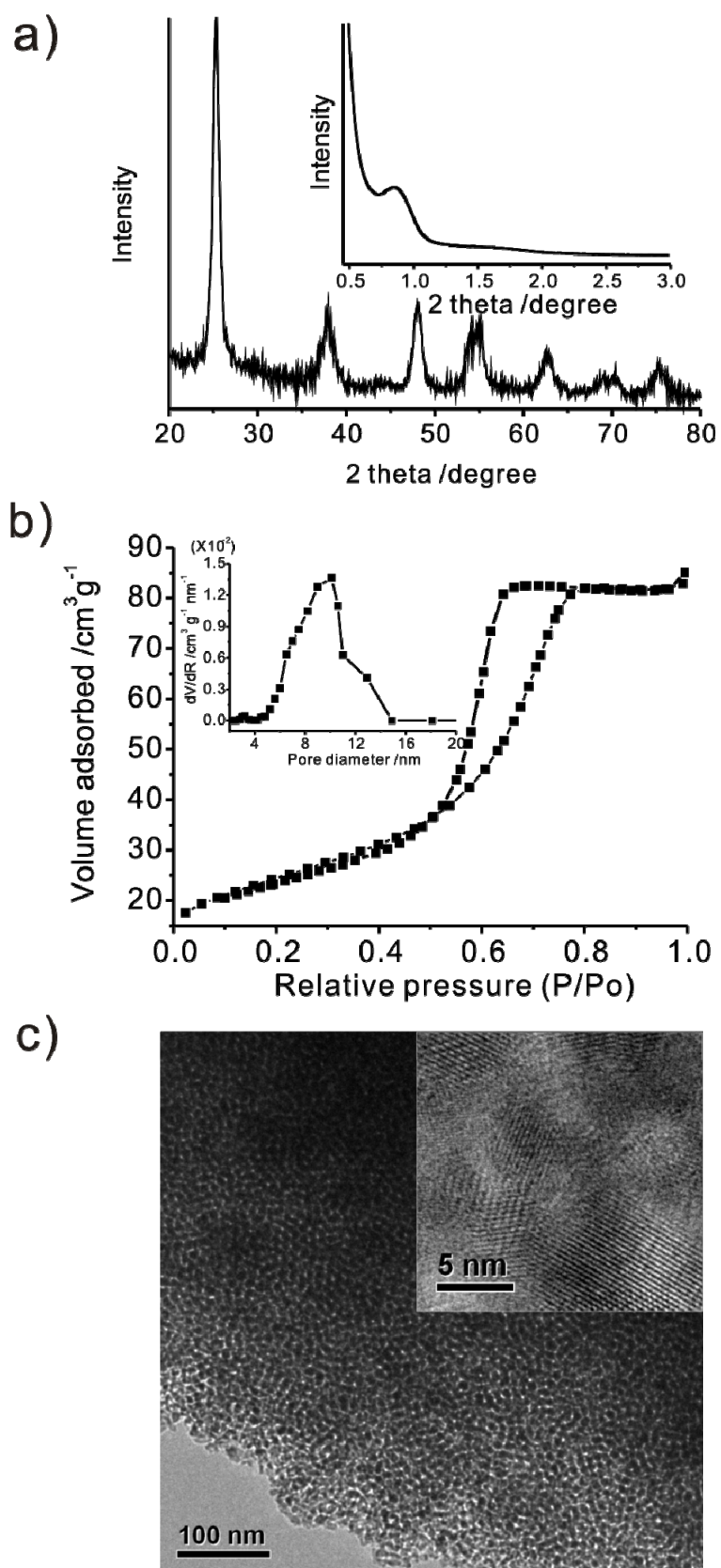5.   D. Vanderbilt, *Phys. Rev. B*, 1990, **41**, 7892-7895.

Figure S1. (a) Wide-angle and small-angle (inset) XRD pattern of mTiO$_2$, (b) N$_2$ adsorption-desorption isotherm and pore size distribution plots (inset, calculated based on BJH model) of mTiO$_2$, and (c) TEM image of mTiO$_2$ (inset is HRTEM image).

The mesoporous materials were calcined at 450 °C in air for 5 h to remove the organic templats and to crystallize the TiO_2 frameworks. The photocatalysts possess one diffraction peak in the low-angle region, indicating the presence of partial mesoscopic periodicity (Figure S1a, inset). It is known that wormhole-like mesostructures often display a single peak in low-angle XRD, which are apparent from TEM observations (Figure S1c). They are less regular in diameter and randomly packing in a three-dimensional manner. Wide-angle XRD analysis (Figure S1a) reveals that the channel walls of $mTiO_2$ consist of nano-sized anatase crystals (JCPDS, No. 21-1272), which is consistent with the high-resolution TEM (HRTEM) image (Figure 1c, inset). Average crystalline size calculated from the broadening of the (101) XRD peak of anatase phase is 11.9 nm. The N_2 adsorption-desorption isotherm and pore size distribution of $mTiO_2$ is shown in Figures S1b. The isotherm is type IV with a H_1 hysteresis loop, which is characteristic of mesoporous materials. The pore size distribution of the sample is broad, and average size is determined to be 10.1 nm. The surface area and pore volume of $mTiO_2$ is 85 m^2/g and 0.13 cm^3/g, respectively.
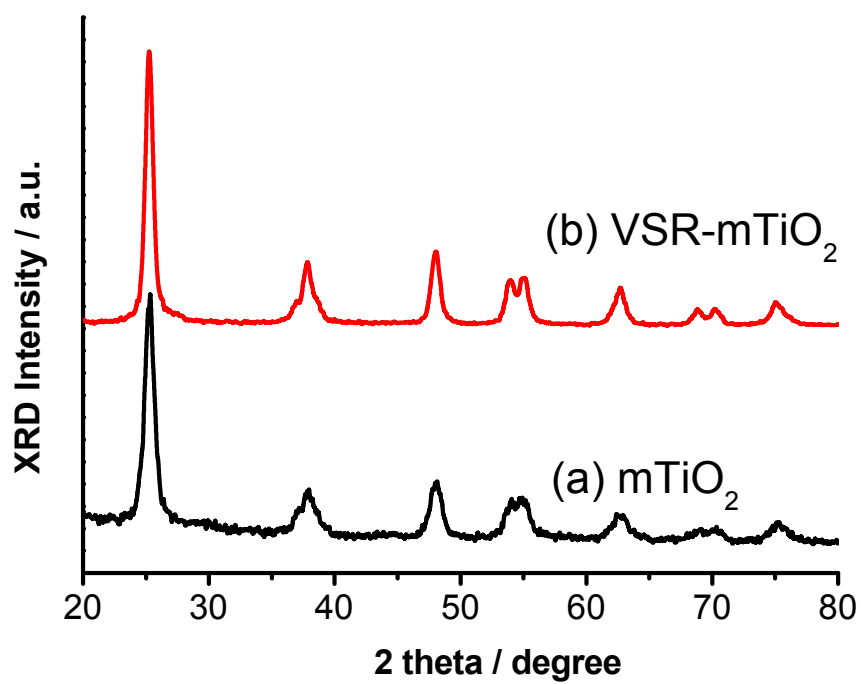
Figure S2. XRD spectra of VSR-mTiO$_2$ and bare mTiO$_2$.
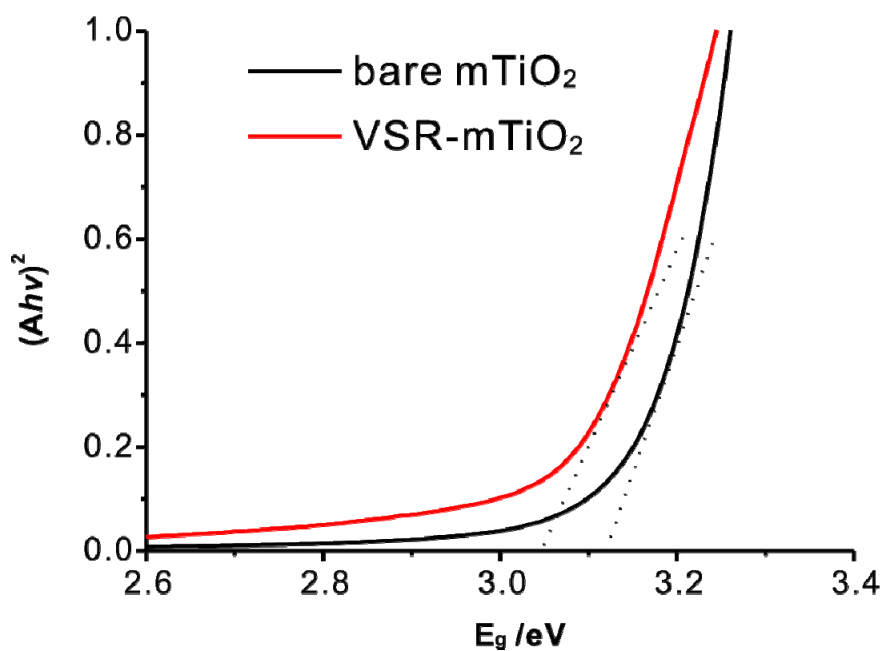
Figure S3. Estimated band gap of VSR-mTiO$_2$ and bare mTiO$_2$.

The optical band gap of bare mTiO$_2$ and VSR-mTiO$_2$ samples were estimated by the following equation (for direct-band-gap materials):

$$(Ahv)^2 = hv - E_g$$

where E$_g$ is the band-gap energy. Plots of (Ahv)^2 versus E$_g$ of the smaples are shown in Figure S1. Extrapolating the lines to the E$_g$ axis, the band-gap energies of bare mTiO$_2$ and VSR-mTiO$_2$ are estimated to be 3.12 and 3.05 eV, respectively.
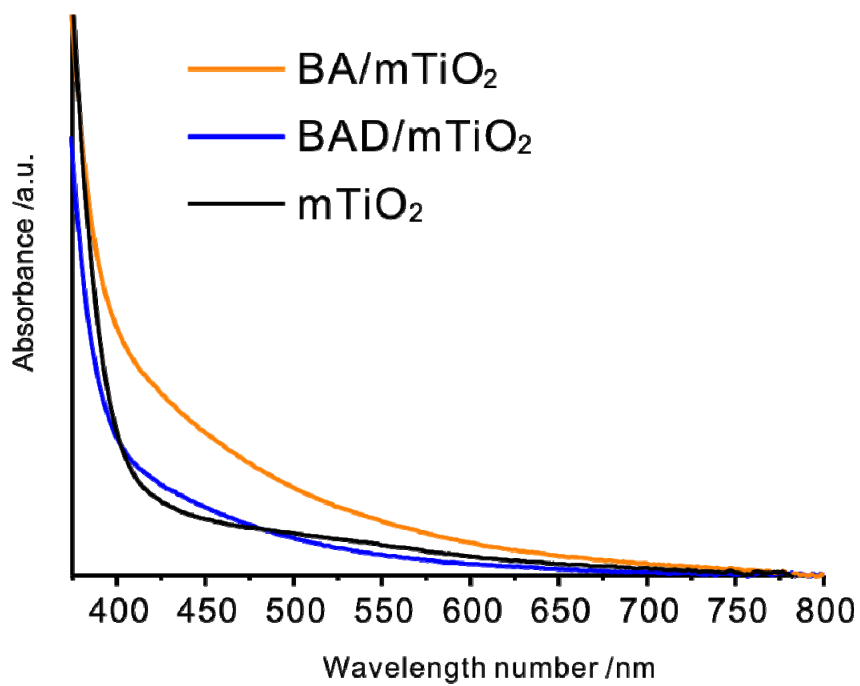
Figure S4. UV/Vis spectra of BA adsorbed $mTiO_2$ ($BA/mTiO_2$), $BAD/mTiO_2$ and $mTiO_2$.
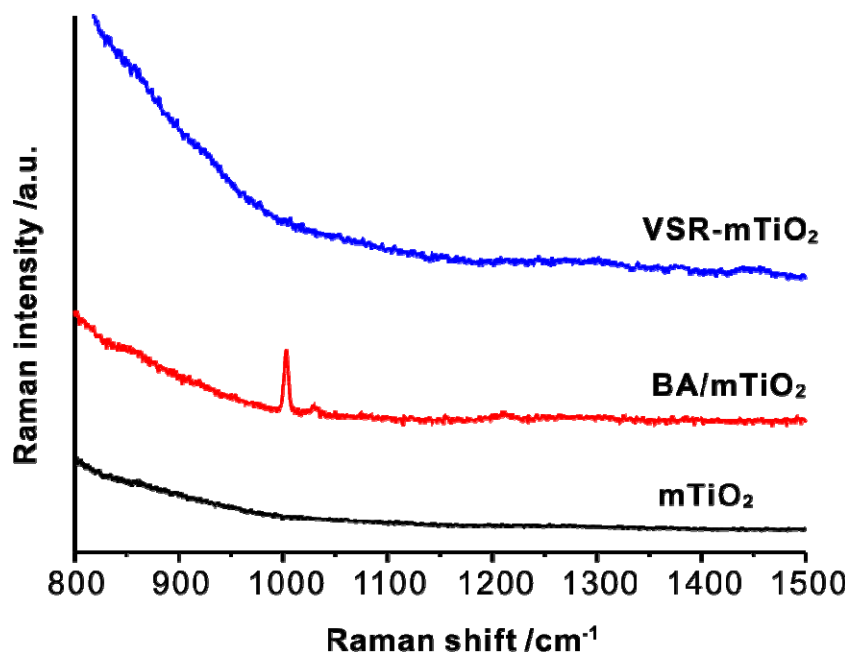
Figure S5. Raman spectra of bare $mTiO_2$, $BA/mTiO_2$ (molar ratio of BA/TiO_2 = 1:200), and $VSR-mTiO_2$; the strong Raman shift at about 1004 cm^{-1} band is attributed to the ring-breathing mode, and no such mode is observed in $VSR-mTiO_2$.
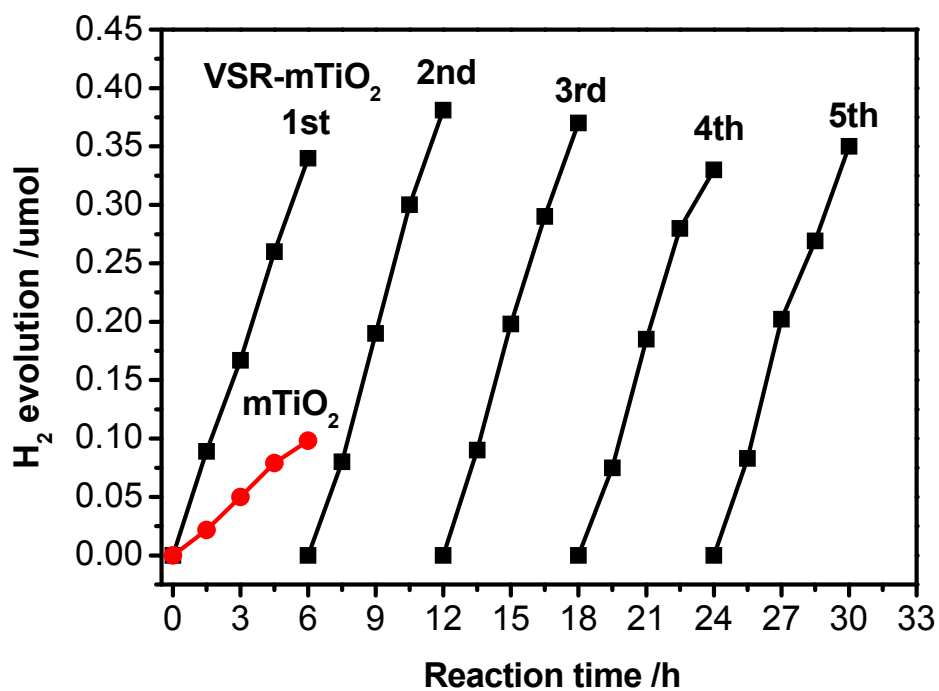
Figure S6. H_2 evolution by formaldehyde decomposition over VSR-mTiO$_2$ and bare mTiO$_2$ under visible-light ($\lambda > 400$ nm), and the repeated experiments.
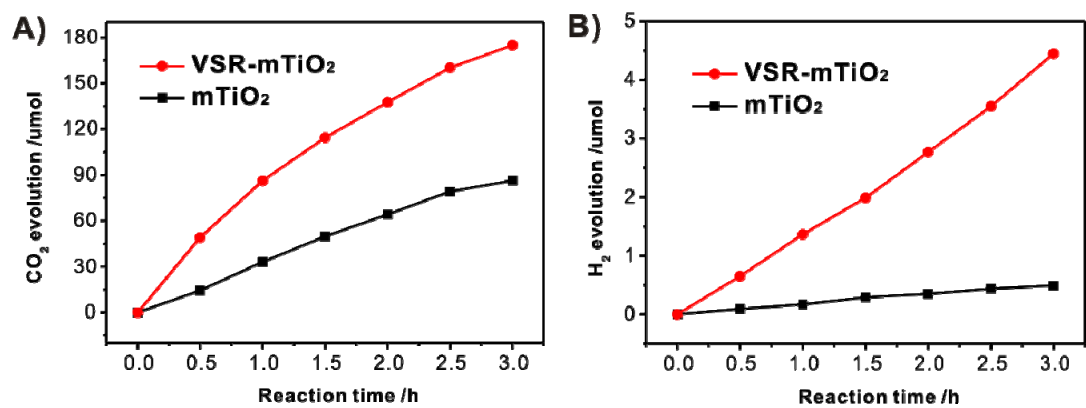
Figure S7. (A) CO_2 and (B) H_2 evolution from formaldehyde solution (5.0 vol%) in the suspension containing VSR-mTiO$_2$ or bare mTiO$_2$ (catalyst amount: 10 mg) under UV light irradiation.
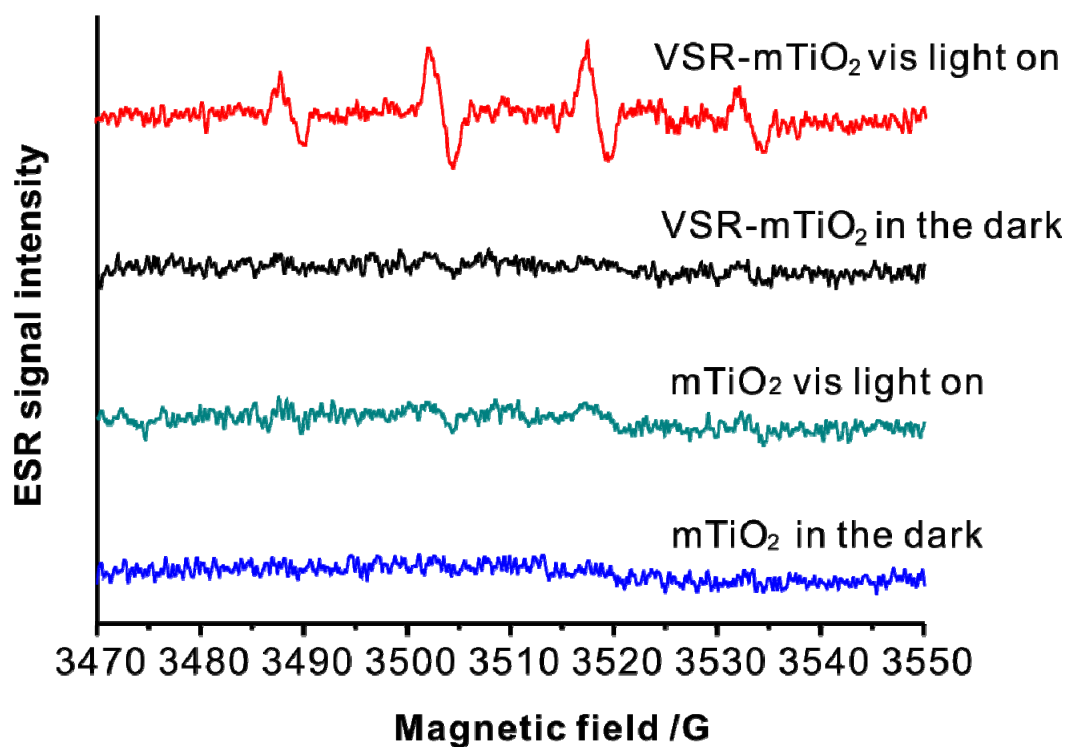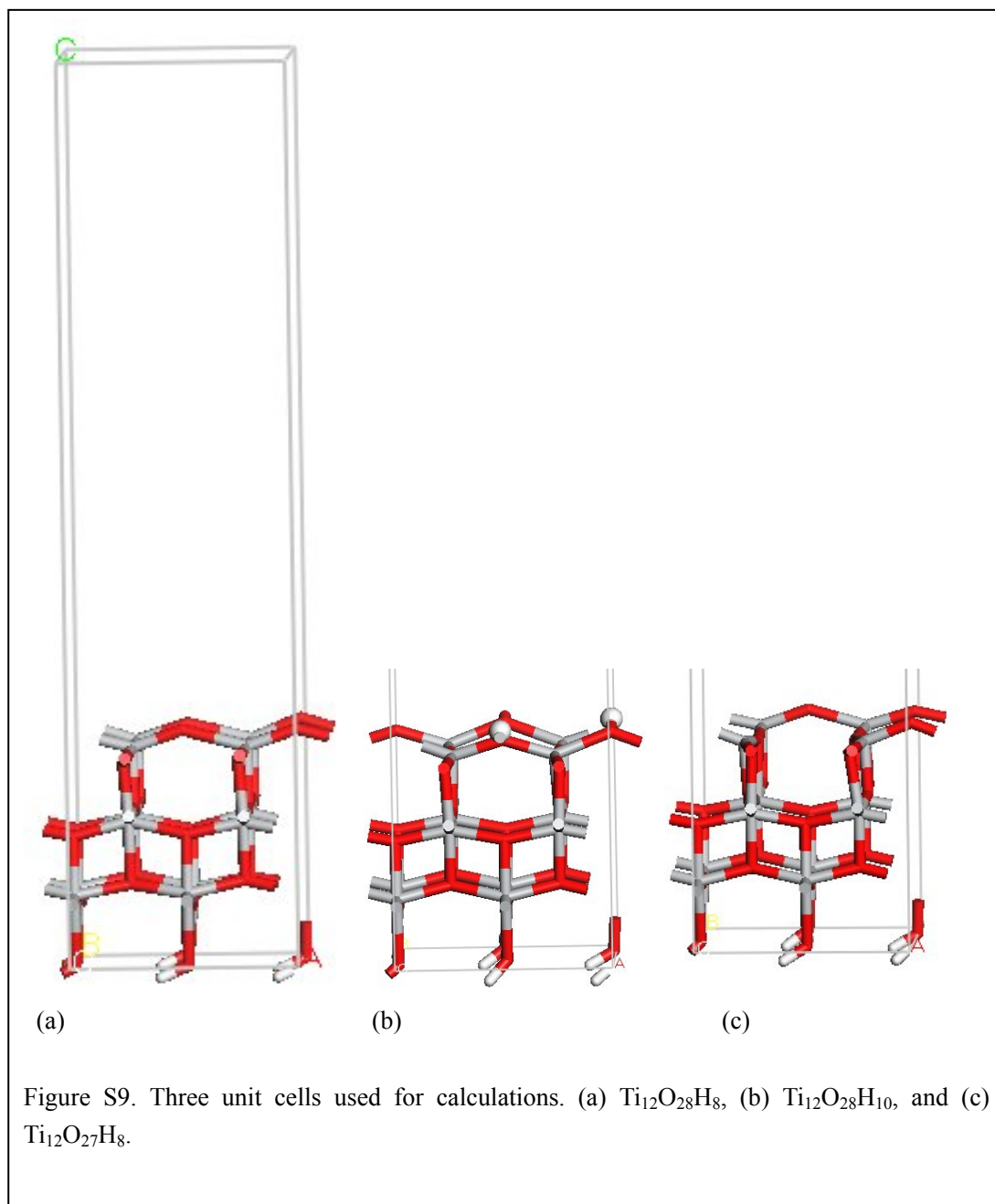
Figure S8. The DMPO-OH· adducts appear only in the suspension of VSR-mTiO$_2$ as soon as visible-light was on.
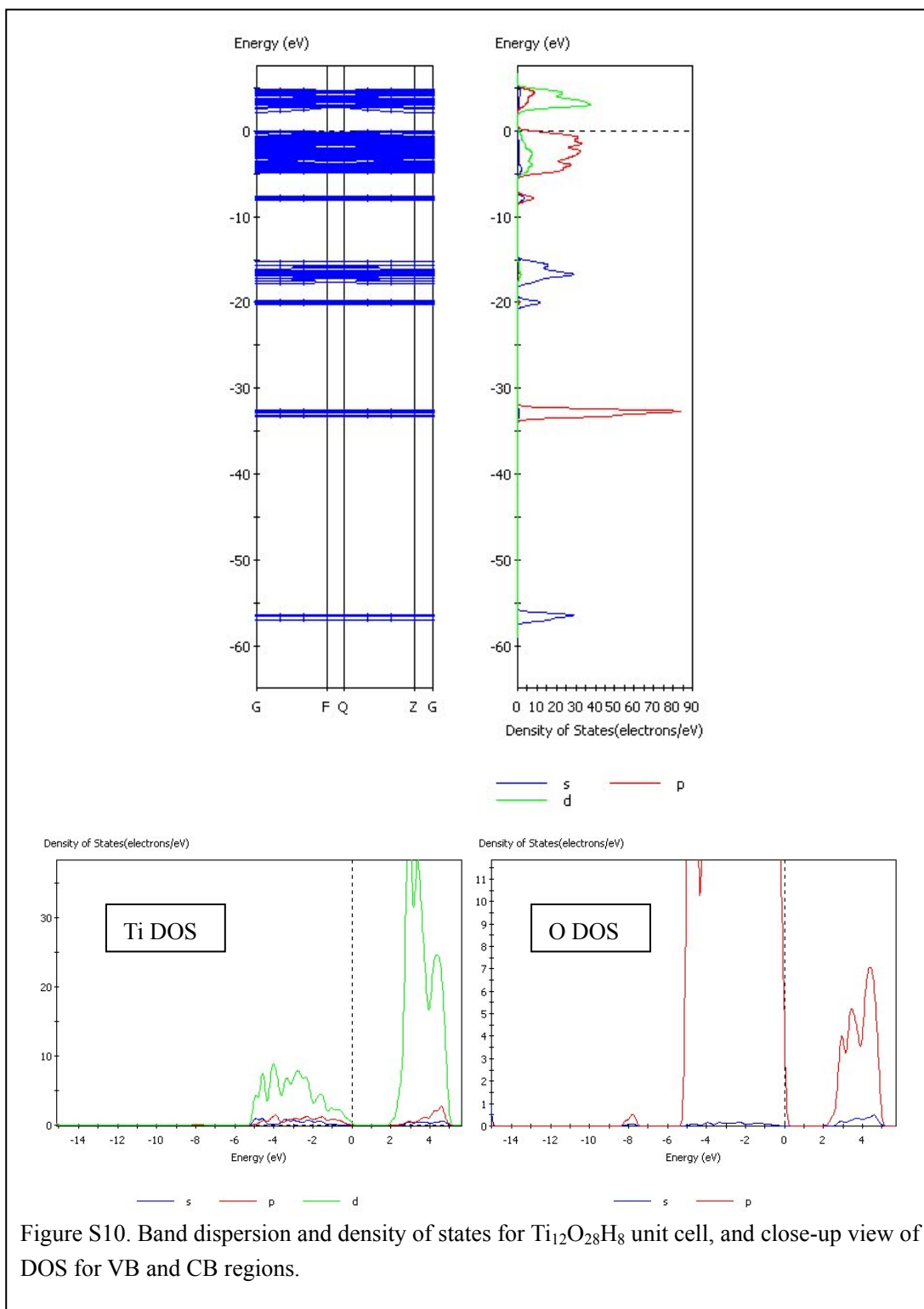
Figure S9. Three unit cells used for calculations. (a) $Ti_{12}O_{28}H_8$, (b) $Ti_{12}O_{28}H_{10}$, and (c) $Ti_{12}O_{27}H_8$.

Figure S10. Band dispersion and density of states for $Ti_{12}O_{28}H_8$ unit cell, and close-up view of DOS for VB and CB regions.
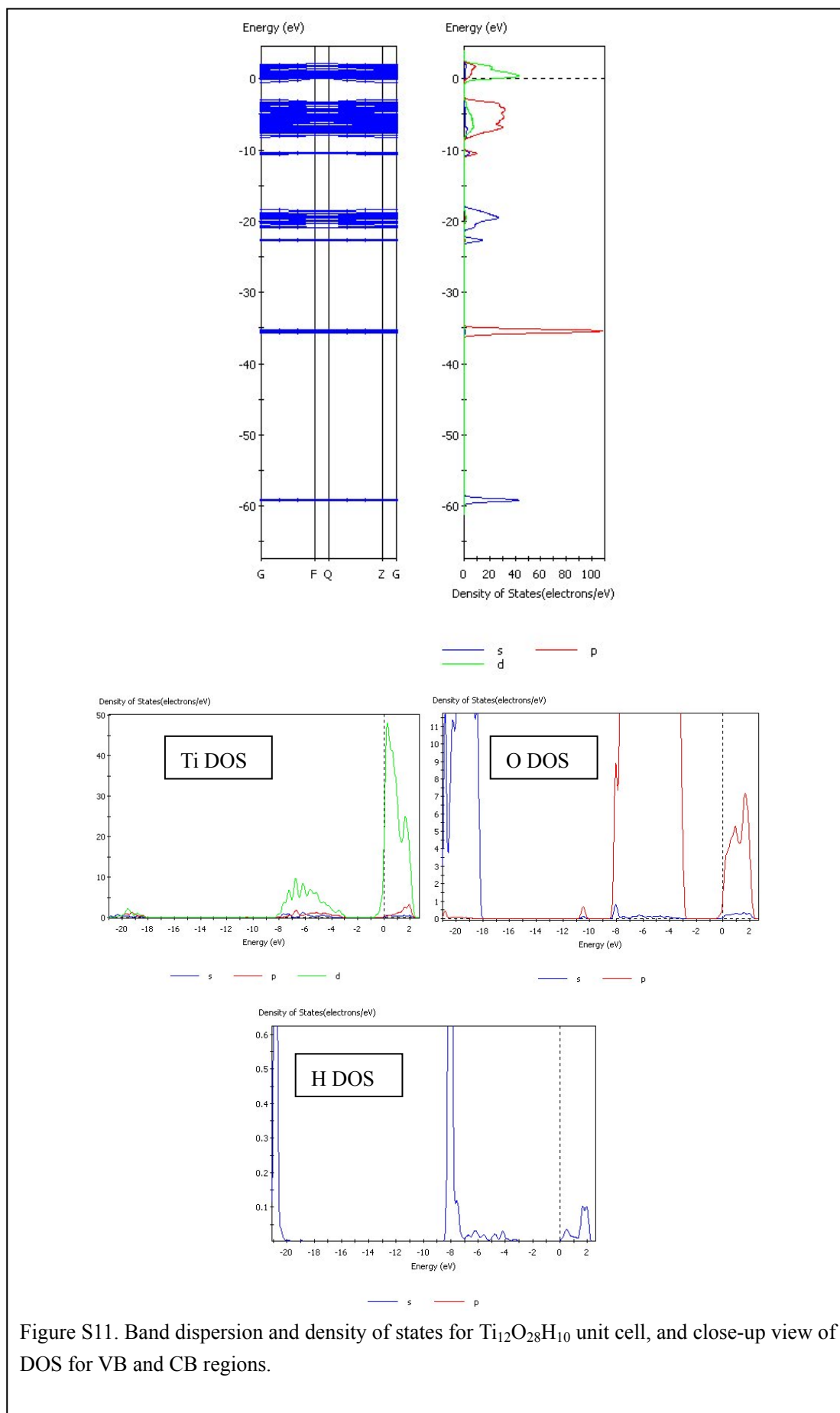
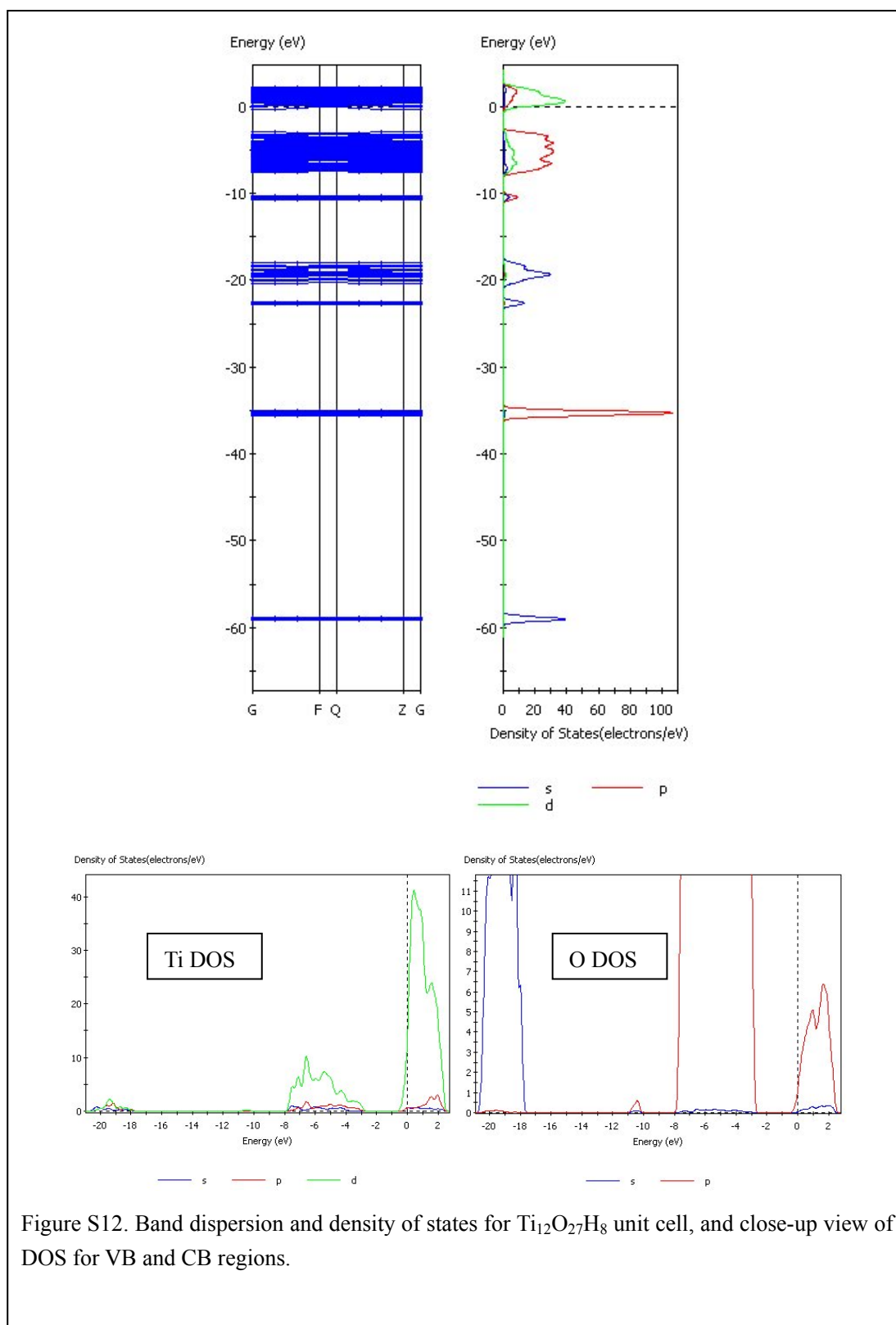Figure S11. Band dispersion and density of states for $Ti_{12}O_{28}H_{10}$ unit cell, and close-up view of DOS for VB and CB regions.

Figure S12. Band dispersion and density of states for $Ti_{12}O_{27}H_8$ unit cell, and close-up view of DOS for VB and CB regions.